Ain Shams Engineering Journal 15 (2024) 103106

Contents lists available at ScienceDirect

Ain Shams Engineering Journal

journal homepage: https://www.sciencedirect.com

Full Length Article

Optimization of thermal performance in hybrid nanofluids for parabolic trough solar collectors using Adams–Bashforth–Moulton method

Anup Kumar [a], Bhupendra K. Sharma [a,*], Taseer Muhammad [b], Laura M. Pérez [c]

[a] Department of Mathematics, Birla Institute of Technology and Science, Pilani, Rajasthan, India
[b] Department of Mathematics, College of Sciences, King Khalid University, Abha 61413, Saudi Arabia
[c] Departamento de Ingeniería Industrial y de Sistemas, Universidad de Tarapacá, Casilla 7D, Arica 1000000, Chile

ARTICLE INFO

Keywords:
Concentric tubes
Thermophoresis and Brownian motion
Hybrid nanofluid
Forth order predictor-corrector-scheme
Solar thermal energy storage

ABSTRACT

Solar energy is an environment-friendly renewable energy source that fulfills the energy consumption requirements of the world economy. Concentrated solar power is the most advanced technology that efficiently absorbs concentrated solar energy. This article investigates the solar energy storage and entropy generation in concentrated parabolic trough solar collectors for hybrid nanofluid flow due to a spinning tube inserted at the receiver's center. The effect of copper nanoparticles and multi-walled carbon nanotube mixture is studied using water-based fluid. Also, the influence of an external magnetic field is investigated with thermophoresis and Brownian motion of nanoparticles. The governing equations for the nanofluid flow are derived using the conservation principles of mass, momentum, energy, and concentration with boundary layer assumptions and no-slip boundary conditions. The governing equations are numerically solved using Adam Bashforth and Adam Moulten's fourth-order predictor-corrector numerical scheme along with the shooting approach. The numerical outcomes for the fluid velocity, temperature, Nusselt number, and entropy formation against various influential physical parameters have been discussed using graphs. It is observed that the augmenting Eckert number, thermophoretic diffusion parameter, and Brownian motion parameter escalates the thermal profiles. Also, an escalation of the radiation parameter and Lewis number enhances the Nusselt number. Thermal energy storage in solar collectors utilizing different terminologies is crucial for improving the efficiency and performance of solar thermal collectors.

1. Introduction

Energy demand is increasing at a very high rate due to industrialization, increasing population, and high living standards. In search of this need, renewable energy sources are preferred due to their sustainability and environment-friendly nature. Solar energy stands at the forefront of renewable energy sources. Solar energy is sustainable, clean, readily available in massive amounts, and not harmful to the environment; it can meet the world's energy needs by adopting efficient technologies. Solar collectors convert solar energy into thermal energy by absorbing radiant energy from sun radiation. Parabolic trough solar collectors are preferred and efficient solar collectors that store concentrated radiant energy from the sun. A parabolic trough is used to reflect and concentrate the solar radiations about a fixed axis, and the solar collectors transform the incoming radiation energy into thermal energy. However, performance enhancement is the primary concern for researchers and scientists in solar thermal collectors to minimize energy loss and maximize the energy storage in the solar collectors. Maximum sunlight absorption and minimum heat dissipation are the primary requirements for improving the performance of solar collectors. Padilla et al. [1] introduced the aspects of heat transport in parabolic trough solar collectors. Jianfeng et al. [2] attempted the enhancement of performance of the receiver tubes in parabolic trough collectors. The absorber or receiver tube is a significant part of the setup of a parabolic trough collector. The collector's overall performance depends upon the receiver tube and heat transfer fluid as discussed by Wang et al. [3]. Chen et al. [4] made a computational model to examine the thermal performance of the receiver tube. Lipinski et al. [5] reviewed the advancements, difficulties, and perspectives of high-temperature thermal energy storage in solar systems. Performance evaluation and cooling system optimization for

* Corresponding author.
E-mail addresses: yadavanupbalwan1996@gmail.com (A. Kumar), bhupen_1402@yahoo.co.in (B.K. Sharma), tasgher@kku.edu.sa (T. Muhammad), lperez@academicos.uta.cl (L.M. Pérez).

https://doi.org/10.1016/j.asej.2024.103106
Received 11 October 2023; Received in revised form 28 June 2024; Accepted 3 October 2024
Available online 4 November 2024

solar panels in Islamabad, Pakistan's climate was done by Sattar et al. [6]. Arifin et al. [7] evaluated the performance of a photovoltaic thermal collector based on nanofluids and with varying convection cooling flows. Sher et al. [8] discussed the impact of humidity and various types of dust on the functionality of renewable energy modules. Some recent studies made to investigate thermal energy storage in solar collectors are [9], [10].

The researcher's primary objective in solar collectors is to maximize radiation absorption and minimize heat loss inside the absorber tube. The external magnetic fields can control fluid flow dynamics having significant electrical conductivity. The applied magnetic field diminishes the flow rate, escalating the radiation absorption by maximizing the contact between the heat transfer fluid and the receiver's tube surface. Kandaswamy et al. [11] analyzed the performance of an incompressible magnetized copper-water nanofluid flow due to solar radiations and demonstrated that a magnetic field controls the fluid flow. Sharma et al. [12] modeled the pulsatile magnetohydrodynamic blood flow with a heat source through the porous medium. Williamson nanofluid flow was examined by Hayat et al. [13] under the effect of melting heat and applied magnetic field. Dinh et al. [14] imposed the magnetic field for heat transfer by the melting surface. Mishra and Sharma [15] studied the mixed convection magnetized flow with the hall effect through the channel. Hsiao [16] used an enhanced parameters effect controlling method to create a system for the extrusion of thermal energy. Tripathi et al. [17] analyzed the two-phase magnetohydrodynamic blood flow with the dependency of viscosity on temperature. Soomro et al. [18] studied the lid-driven triangular cavity filled with water for convection heat transfer. Magnetohydrodynamic liquid metal technology applications in the generation of solar power were described by Deng et al. [19]. Al-Cruz et al. [20] comprehensively analyzed the entropy generation due to the phase change material in the magnetohydrodynamic spinning cylinder. Ghandhi et al. [21] did the modeling of drug delivery for the hybrid nanoparticles in a magnetized occluded artery with varying viscosity. Khanduri et al. [22] studied the electroosmotic magnetized hydrodynamic flow with thrombosis through a curve artery. Sharma and Gandhi [23] introduced the time-dependent magnetohydrodynamic flow driven by the mixed convection under the effect of a nonuniform heat source. Sharma et al. [24] discussed the Jeffrey electromagnetohydrodynamic nanofluid flow for solar energy applications, analyzing heat and mass transfer along variably thicked surfaces. Some other recent investigations made for the study of magnetohydrodynamic flows [25], [26]. Adjusting the turbulator layout affects the tubular heat exchanger's heat transmission and hydraulic performance as studied by Ahmadi [27]. Ji et al. [28] studied the influence of a spiral elastic tube heat exchanger's deflector orientation on heat transfer capacity.

The most effective Brownian motion theory has been applied to the nanofluid models to introduce the thermal conversion system of nanofluids. The influences of thermophoresis and Brownian motion with the influence of solar radiation were studied by Ghasemi et al. [29]. Thermophoresis is a phenomenon caused by the floating of nanoparticles in the non-isothermal system in response to the thermal gradient. These nanoparticles scatter the incident radiation, which increases the radiation absorption in the receiver tube. The random motion of nanoparticles in the liquid is known as the Brownian motion. The random motion of particles undergoes collision, and these collisions entail energy transfer between particles. Brownian motion of the suspended nanoparticles within the base fluids is the mechanism for the abnormal enhancement in the thermal conductivity of nanofluid's. Anbuchezhian et al. [30] discussed the boundary layer nanofluid flow due to thermal stratification with thermophoresis and Brownian motion and this study extended by Kandaswamy et al. [31] to magnetohydrodynamic nanofluid flow. Shehzad et al. [32] demonstrated a model for solar energy with Brownian motion and thermophoresis of nanoparticles. Patel and Singh [33] examined the microplanar nanofluid flow with the Brownian motion and thermophoresis under the effect of thermal radiation. Nayak et al. [34] developed a combined approach for the heat transfer in the receiver tube with thermophoresis and Brownian motion to intensify the heat transport. Solar energy applications for the influence of thermophoresis in heat transfer for diverse geometries due to nanofluid flow were analyzed by Rekha et al. [35]. Sharma et al. [36] studied the heat transport of the nanofluid flow over-stretching surface with the thermophoresis and Brownian motion of the nanoparticles.

The fundamentals of entropy generation in fluid flows for energy storage systems were described by Bejan [37]. Heat transfer in solar collectors by thermofluidic processes undergoes some irreversibilities, resulting in an efficiency loss as explained by Boer and Tamm [38]. Minimizing entropy generation in thermal storage systems is essential because it improves any device or system's functionality, performance, and efficiency. In practice, the entropy generation rate determines the quantity of irreversibilities. Oztop and Salem [39] reviewed the entropy generation in energy conversion and storage systems by mixed or natural convection heat transfer. Improvements to the geometry of thermal energy storage using shell and tube technology for latent heat analyzing entropy generation were done by Guelpa et al. [40]. Thermal systems with entropy measures to sustainably use renewable energy technologies as studied by Khan et al. [41]. The heat transmission in a miniature linear Fresnel prototype using hybrid nanofluids ($rGO - Co_3O_4$/water) was studied by Said et al. [42]. Sharma et al. [43] did the study of entropy formation optimization in higher-order chemical reaction for the magnetohydrodynamic flow. Ghandhi et al. [44] studied the entropy formation in magnetized hybrid nanofluid blood flow for hemodynamical applications. Kumawat et al. [45] done the entropy analysis of a magnetized curve-shaped artery with mass and heat transport by simulating two-phase flow. Tavakoli et al. [46] used phase change material and sinusoidal internal fins simultaneously to exhibit thermohydraulic performance in LHTES systems. Lead acid battery state of charge prediction for cutting edge renewable energy systems with neural networks was done by Widjaja et al. [47].

In the literature mentioned above, many attempts have been made to analyze the heat transfer due to magnetized nanofluid flows over various stretching surfaces and cylindrical pipes. From the literature survey, it is noticed that no attempt has been made to describe the effect of a rotating tube inserted at the center of the absorber tube in solar collectors under thermophoretic diffusion and Brownian motion of the hybrid nanoparticles to maximize the radiation absorption by the working fluid. The rotational effect of the inner tube will generate disturbance in the nanofluid flow and enhance the fluid mixing, which will result in enhanced radiation absorption from sunlight, which, in turn, improves the performance of the solar collectors. Therefore, this attempt studied the heat transfer in parabolic trough solar collectors for the hybrid nanofluid flow due to an applied magnetic field under the effect of a rotating tube with thermophoresis and Brownian motion of nanoparticles. To fill the gaps mentioned above, the main remarks and novelty of this attempt are:

- An advanced type of hybrid nanoparticles, Copper and Multiwalled carbon nanotubes, are used in the analysis to improve the conductive properties of heat transfer fluid.
- Water is used as the heat transfer fluid in the investigation because water is readily available having low viscosity and higher thermal capacity.
- Influences of thermophoretic diffusion and Brownian motion are encountered to analyze the nanoparticle's movement in response to the thermal gradient.
- The impact of the external magnetic field produces a parallel Lorentz force that controls flow dynamics by affecting the drag coefficient.
- Optimized heat transfer is examined in the receiver tube under the influence of an inserted rotating cylinder in the center of the absorber tube. The rotating cylinder increases the movement of fluid

particles in the hybrid nanofluid, enhancing internal heat absorption.
- Entropy generation is also studied to estimate the irreversibilities generated in the heat transfer.

Energy demand rapidly increases due to industrialization, population growth, and rising living standards. Renewable energy sources are ideal for meeting this need because of their sustainability and environmental friendliness. Solar energy is the perfect renewable energy source as it is clean, readily available, and environmentally friendly. Concentrated solar power technology is used to collect solar energy from sunlight and is known as a solar thermal collector. Enhancement of the performance of solar collectors is the primary concern for researchers to maximize thermal energy storage and minimize energy loss. Therefore, this attempt is made to enhance the performance of solar collectors by introducing novel concepts and assumptions. This attempt addresses the influence of the rotating tube inserted at the center of the receiver tube in the presence of the external magnetic field for the hybrid nanofluid flow. The rotational effect of the inner tube inserted at the center of the receiver tube will generate disturbance in the fluid flow and fluid mixing in the boundary layer, which results in efficient heat transfer. Additionally, the applied magnetic field will develop the parallel Lorentz force, which will minimize the drag coefficient at the receiver's tube surface. This resistance increases the contact between the fluid flow and the absorber tube, which enhances radiation absorption. The hybrid nanoparticles in water will advance the heat transfer fluid by advancing the physical properties of the base fluid. This article has been divided into seven essential subsections. A detailed explanation of these subsections or the article structure is described below:

- The first part contains the introduction section, which briefly analyzes the existing literature and the gaps available in the literature.
- The second part is the physical assumption section; this section contains the physical assumptions considered toward the advancement of concentrated solar power technology and terminologies considered for the mathematical modeling of the governing equations.
- The third section contains the numerical procedure used to simulate the governing equations to find numerical outcomes.
- The fourth section presents the validation and analysis of the numerical results obtained from applying the numerical methodology.
- Section five describes the quantity of engineering interest and the corresponding outcomes.
- Section six is the entropy optimization section, which explains the terminologies involved in the entropy generation and their corresponding outputs.
- Finally, section seven presents the concluded remarks of the study.

2. Physical assumptions

The time-independent boundary layer hybrid nanofluid flow between concentric tubes with the influences of viscous dissipation, thermophoretic diffusion, Brownian motion, and Ohmic heating with no-slip boundary conditions is assumed. The non-uniform radiative heat flux distribution on the tube is assumed from the concentrated solar radiations reflected by the parabolic trough about the receiver tube placed at a focal length of the trough. A mixture of Multi-walled carbon nanotubes and Copper nanoparticles with water is considered the heat transfer fluid. Hybrid nanofluid flow is considered as symmetrical along the axial and angular directions. R is the radial direction with velocity components U. The physical geometry of the solar collector is presented in Fig. 1.

In the case of electrically conductive fluid flow, the magnitude of current density produced by the magnetic field is sufficient to control the fluid flow. Therefore, the current density generated due to the external

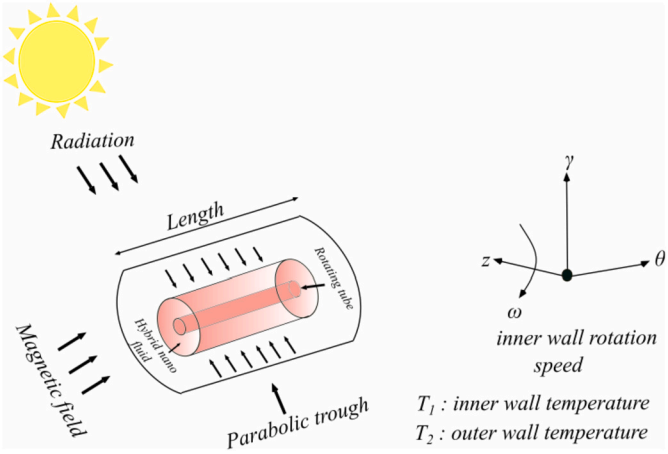

Fig. 1. Physical geometry of the solar collector.

magnetic field is $J = \sigma(B \times U)$, and the Lorentz force is $F = \sigma(B \times U) \times B$.

Nanofluid flow is assumed as the steady, laminar, and unidirectional. Thus, the fluid velocity and velocity gradients in the angular and axial directions with respect to α and z vanishes. In this case, the equations governing the fluid flow are [48], [49]:

Governing equations:

Continuity equation:

$$\frac{\partial(RU)}{\partial R} = 0, \tag{1}$$

Momentum equation:

$$U\frac{\partial U}{\partial R} = \nu_{hnf}\left(\frac{\partial^2 U}{\partial R^2} + \frac{1}{R}\frac{\partial U}{\partial R} - \frac{U}{R^2}\right) - \frac{\sigma_{hnf} U B^2}{\rho_{hnf}}, \tag{2}$$

Energy equation:

$$\begin{aligned}\left(\rho C_p\right)_{hnf} U\frac{\partial T}{\partial R} = {} & \frac{k_{hnf}}{R}\frac{\partial}{\partial R}\left(R\frac{\partial T}{\partial R}\right) \\ & + \tau\left[D_B\frac{\partial T}{\partial R}\frac{\partial C}{\partial R} + \frac{D_T}{T_\infty}\left(\frac{\partial T}{\partial R}\right)^2\right] \\ & + \mu_{hnf}\left(\frac{\partial U}{\partial R} - \frac{U}{R}\right)^2 - \frac{\partial R q_r}{\partial R},\end{aligned} \tag{3}$$

where,

$$q_r = -\frac{4\sigma_e}{3\beta_R}\frac{\partial T^4}{\partial R}, T^4 \cong 4T_2^3 T - 3T_2^4.$$

Concentration equation:

$$U\frac{\partial C}{\partial R} = D_B\left[\frac{1}{R}\frac{\partial C}{\partial R} + \frac{\partial^2 C}{\partial R^2}\right] + \frac{D_T}{T_\infty}\left[\frac{1}{R}\frac{\partial T}{\partial R} + \frac{\partial^2 T}{\partial R^2}\right], \tag{4}$$

Boundary conditions:

$$\begin{cases} R = r_1: & U(R) = \omega r_1, \quad T = T_1, \quad C = C_1, \\ R = r_2: & U(R) = 0, \quad T = T_2, \quad C = C_2. \end{cases} \tag{5}$$

where, the equation (1) is the continuity equation for one-dimensional steady-state hybrid nanofluid flow which preserve mass conservation principle, equation (2) is momentum equation representing velocity distribution in the fluid flow with convection, diffusion and magnetic field terms, equation (3) is the energy equation representing the thermal distribution in the hybrid nanofluid flow due to the convection, diffusion, viscous dissipation, thermophoretic diffusion, Brownian motion and radiation heat transfer, equation (4) is the concentration equation governed by convection, diffusion, thermophoretic diffusion, and Brownian

motion, and equation (5) represents the no-slip boundary conditions, q_r is the non-uniform radiative heat flux distribution estimated by the Rosseland approximation, ν_{hnf} is the kinematic viscosity, r_1 is the radius of the inner tube, T_2 is the surface temperature of the inner rotating tube, C_2 is the nanoparticle concentration at the inner tube, k_{hnf} is the thermal conductivity, D_T is the thermophoresis diffusion, β_R is the absorption coefficient, μ_{hnf} is the dynamic viscosity, σ_e is the Stefan-Boltzmann constant, D_B is the coefficient of Brownian diffusion, r_2 is the radius of the outer tube, T_1 is the surface temperature of the outer tube, ω is the speed of angular rotation, and C_1 is the nanoparticles concentration at the surface of the outer tube. Relations used for the calculation of thermal properties of hybrid nanofluids are:

Dynamic viscosity

$$\mu_{hnf} = \frac{\mu_f}{\left(1-\phi_1\right)^{2.5}\left(1-\phi_2\right)^{2.5}},$$

Density

$$\rho_{hnf} = \phi_1\rho_1 + \left(1-\phi_1\right)\left[\left(1-\phi_2\right)\rho_f + \phi_2\rho_2\right],$$

Specific heat capacity

$$(c_p)_{hnf} = (1-\phi_1)[\left(1-\phi_2\right)(c_p)_f + \phi_2(c_p)_2] + \phi_1(c_p)_1,$$

Thermal conductivity

$$k_{hnf} = \left(k_{nf}\right) \times \frac{k_1 + 2k_{nf} - 2\phi_1\left(k_{nf}-k_1\right)}{\phi_1(k_{nf}-k_1) + k_1 + 2k_{nf}},$$

where

$$k_{nf} = \frac{k_2 + 2k_f - 2\phi_2\left(k_f - k_2\right)}{k_2 + 2k_f + \phi_2\left(k_f - k_2\right)} \times \left(k_f\right),$$

Elecrical conductivity

$$\sigma_{hnf} = \left(1 + \frac{3(\sigma_1 - \sigma_{nf})\phi_1}{(\sigma_1 - 2\sigma_{nf}) - (\sigma_1 - \sigma_{nf})\phi_1}\right)\sigma_{nf}$$

where

$$\sigma_{nf} = \left(1 + \frac{3(\sigma_2 - \sigma_f)\phi_2}{(\sigma_2 - 2\sigma_f) - (\sigma_2 - \sigma_f)\phi_2}\right)\sigma_f$$

Physical Properties	Copper	MWCNT	Water
Thermal Conductivity [κ (W/mK)]	401	3000	0.613
Electrical conductivity [S/m]	5.96×10^7	1.9×10^{-4}	0.05
Heat Capacitance [C_p (J/kgK)]	385	796	4179
Density [ρ (kg/m^3)]	8933	1600	997

Above governing equation are non-dimensionalized by employing the following appropriate dimensionless variables:

$$r = \frac{R}{r_2}, \quad u = \frac{U}{\omega r_1}, \quad \eta = \frac{r_1}{r_2}, \quad \theta = \frac{T-T_2}{T_1-T_2}, \quad \theta = \frac{C-C_2}{C_1-C_2}.$$

Dimensionless governing equations:

Momentum equation:

$$\frac{d^2u(r)}{dr^2} + \frac{1}{r}\frac{du(r)}{dr} - \left\{\frac{M^2}{\left(1-\eta^2\right)}\frac{S_5}{S_2} + \frac{1}{r^2}\right\}u(r) - Re\frac{S_1}{S_2}u(r)\frac{du(r)}{dr} = 0, \tag{6}$$

Energy equation:

$$\frac{d^2\theta(r)}{dr^2} + \frac{1}{r}\frac{d\theta(r)}{dr} + EcPr\frac{S_2}{S_4}\left\{\frac{du(r)}{dr} - \frac{1}{r}u(r)\right\}^2 + \frac{4Rd}{3S_4}\frac{1}{r}\frac{d(r\theta(r))}{dr} - PrRe\frac{S_3}{S_4}u(r)\frac{d\theta(r)}{dr} + PrNb\frac{d\theta(r)}{dr}\frac{d\phi(r)}{dr} + PrNt\left(\frac{d\theta(r)}{dr}\right)^2 = 0, \tag{7}$$

Concentration equation:

$$\frac{d^2\phi(r)}{dr^2} + \frac{1}{r}\frac{d\phi(r)}{dr} + \frac{Nt}{Nb}\left[\frac{d^2\theta(r)}{dr^2} + \frac{1}{r}\frac{d\theta(r)}{dr}\right] - RePrLeu(r)\frac{d\phi(r)}{dr} = 0, \tag{8}$$

Boundary conditions:

$$\begin{aligned} r=\eta: &\quad u=1, \quad \theta=1, \quad \phi=1,\\ r=1: &\quad u=0, \quad \theta=0, \quad \phi=0. \end{aligned}$$

where, $Re = \frac{\rho_f\omega r_1 r_2}{\mu_f}$ is the Reynolds number, $Pr = \frac{\mu_f(\rho C_p)_f}{\rho_f k_f}$ is the Prandtl number, $Ec = \frac{\rho_f(\omega r_1)^2}{(\rho C_p)_f \Delta T}$ is the Eckert number, $Rd = \frac{4\sigma_e T_c^3}{\beta_R k_f}$ is the radiation parameter, $M = B_0 d\sqrt{\frac{\sigma_f}{\mu_f}}$ is the magnetic field parameter, $Nb = \frac{D_B(C_1-C_2)}{\nu_f}$ is the Brownian motion parameter, $Nt = \tau\frac{D_T(T_1-T_2)}{\nu_f T_2}$ is the thermophoretic diffusion parameter, $Le = \frac{\alpha}{D_B}$ is the Lewis number, and $S_1 = \frac{\rho_{hnf}}{\rho_f}, S_2 = \frac{\mu_{hnf}}{\mu_f}, S_3 = \frac{(\rho C_p)_{hnf}}{(\rho C_p)_f}, S_4 = \frac{k_{hnf}}{k_f}, S_5 = \frac{\sigma_{hnf}}{\sigma_f}$ are some constants associated with physical properties of the hybrid nanofluids.

3. Numerical procedure

In the numerical procedure, the first-order differential equation system is made after introducing the dimensionless variables; the resulting equations are numerically solved by Adam Bashforth and Adams Moulten's fourth-order predictor-corrector numerical scheme. The system of first-order ordinary differential equations is given by:

Governing equations in the system of differential equations:

$$\begin{aligned}
&u' = u_1,\\
&u_2 = u_1' = -\frac{1}{r}u_1 + \left\{\frac{M^2}{\left(1-\eta^2\right)}\frac{S_5}{S_2} + \frac{1}{r^2}\right\}u + Re\frac{S_1}{S_2}uu_1,\\
&\theta' = \theta_1,\\
&\theta_2 = \theta_1' = \frac{1}{1+4Rd/3S_4}\left[PrRe\frac{S_3}{S_4}u\theta_1 - \frac{1}{r}\theta_1 - \frac{S_2}{S_4}EcPr\left[u_1 - \frac{1}{r}u\right]^2 + PrNb\theta_1\phi_1 + PrNt\theta_1^2 + \left(1+\frac{4Rd}{3S_4}\right)\frac{1}{r}\theta_1\right].\\
&\phi' = \phi_1,\\
&\phi_2 = \phi_1' = RePrLeu\phi_1 - \frac{\phi_1}{r} - \frac{Nt}{Nb}\left[\theta_2 + \frac{\theta_1}{r}\right].
\end{aligned} \tag{9}$$

Boundary conditions:

$$\begin{aligned} r=\eta: &\quad u=1, \quad \theta=1, \quad \phi=1,\\ r=1: &\quad u=0, \quad \theta=0, \quad \phi=0. \end{aligned}$$

The derived differential system for the unknown variables, $u(r), \theta(r)$ and $\phi(r)$, presented in the general form is given below:

$$\begin{aligned}
&\frac{du}{dr} = q(r,u), \quad f\left(r_0\right) = u_0,\\
&\frac{d\theta}{dr} = q(r,\theta), \quad \theta\left(r_0\right) = \theta_0,\\
&\frac{d\phi}{dr} = q(r,\phi), \quad \phi\left(r_0\right) = \phi_0.
\end{aligned}$$

Successive approximation for four step Adam Bashforth explicit (predictor) numerical scheme is given by:

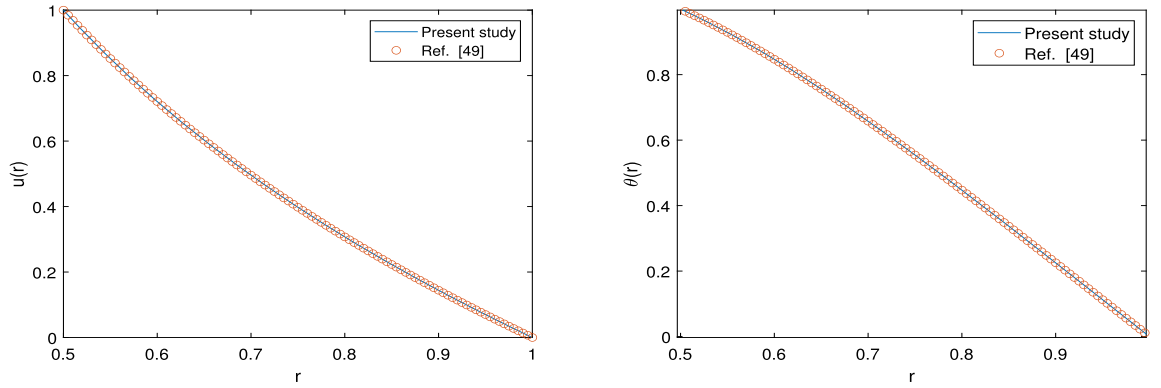

(a) Validation plot for the velocity profiles (b) Validation plots for the temperature profiles

Fig. 2. Validation of this study with the existing literature [49].

$$\begin{aligned}
u_{k+1} &= u_k + \frac{h}{24}[55q(r_k,u_k) - 59q(r_{k-1},u_{k-1}) + 37q(u_{k-2},u_{k-2}) \\
&\quad - 9q(r_{k-3},u_{k-3})], \\
\theta_{k+1} &= \theta_k + \frac{h}{24}[55q(r_k,\theta_k) - 59q(r_{k-1},\theta_{k-1}) + 37q(r_{k-2},\theta_{k-2}) \\
&\quad - 9q(r_{k-3},\theta_{k-3})], \\
\phi_{k+1} &= \phi_k + \frac{h}{24}[55q(r_k,\phi_k) - 59q(r_{k-1},\phi_{k-1}) + 37q(r_{k-2},\phi_{k-2}) \\
&\quad - 9q(r_{k-3},\phi_{k-3})].
\end{aligned} \tag{10}$$

Successive approximation for four step Adams Moulten implicit (corrector) numerical scheme is given by:

$$\begin{aligned}
u_{k+1} &= u_k + \frac{h}{720}[251q(r_{k+1},u_{k+1}) + 646q(r_k,u_k) - 264q(r_{k-1},u_{k-1}) \\
&\quad + 106q(r_{k-2},u_{k-2}) - 19q(r_{k-3},u_{k-3})], \\
\theta_{k+1} &= \theta_k + \frac{h}{720}[251q(r_{k+1},\theta_{k+1}) + 646q(r_k,\theta_k) - 264q(r_{k-1},\theta_{k-1}) \\
&\quad + 106q(r_{k-2},\theta_{k-2}) - 19q(r_{k-3},\theta_{k-3})], \\
\phi_{k+1} &= \phi_k + \frac{h}{720}[251q(r_{k+1},\phi_{k+1}) + 646q(r_k,\phi_k) - 264q(r_{k-1},\phi_{k-1}) \\
&\quad + 106q(r_{k-2},\phi_{k-2}) - 19q(r_{k-3},\phi_{k-3})].
\end{aligned} \tag{11}$$

where k varies from 4 to n, this predictor-corrector method is the four-step numerical approach; therefore, we need the first four steps to solve this system of equations to implement this four-step predictor-corrector method and these first four steps are evaluated by the Runga-Kutta fourth-order numerical scheme.

The momentum, temperature, and concentration equations are all second-order differential equations, necessitating two initial conditions for their numerical solution. However, we currently possess only a single initial condition for each of these equations. To overcome this barrier, the unknown initial conditions for u_1, θ_1 and ϕ_1 are calculated with the shooting method by taking initial guesses t_1, g_1 and m_1. Newton's method update the initial guesses until the solution reaches a desired error tolerance of 10^{-6}. The expression of Newton method to update initial guesses is:

$$t_1 = t_1 - \frac{u(b,n+1) - u(b)}{u_1(b,n+1)},$$

$$g_1 = g_1 - \frac{\theta(b,n+1) - \theta(b)}{\theta_1(b,n+1)},$$

$$m_1 = m_1 - \frac{\phi(b,n+1) - \phi(b)}{\phi_1(b,n+1)},$$

. The calculated values from the numerical scheme at the endpoint are denoted by $u(b,n+1)$, $u_1(b,n+1)$, $\theta(b,n+1)$, $\theta_1(b,n+1)$, $\phi(b,n+1)$, and $\phi_1(b,n+1)$, while the boundary conditions at the domain's endpoint are indicated by $u(b)$, $\theta(b)$ and $\phi(b)$. The initial estimates for momentum. energy, and concentration equations are updated repeatedly with Newton method until the numerical solution converges to the error tolerance of 10^{-6}.

$$u(b,n+1) - u(b) \le 10^{-6},$$

$$\theta(b,n+1) - \theta(b) \le 10^{-6},$$

$$\phi(b,n+1) - \phi(b) \le 10^{-6}.$$

4. Graphical results

This section discusses the numerical outcomes obtained from applying the above methodology against the effective physical parameters for the momentum profile, temperature profile, Nusselt number, and entropy formation. It is necessary to validate the outcomes of this study with the existing one. The current investigation is validated by neglecting this study's novel parameters and assumptions. Fig. 2 represents the validation plots of this analysis with the existing literature [49]. Moreover, it is seen that the performance of the numerical results from the current methodology is in excellent agreement.

Figs. 3(a) and 3(b) report the effects of Reynolds number (Re) and magnetic field parameters (M) on the velocity distribution of the hybrid nanofluids in the boundary layer. Fig. 3(a) demonstrates that the fluid's velocity raises with the increase in the Re. Re is the ratio of a inertial and viscous forces of the fluid. Therefore, the higher Re means the inertial forces become more dominant over viscous forces in the nanofluid flow, and inertial forces occur due to the momentum of fluid particles in the boundary layer. Thus, increasing the momentum of fluid particles for escalating the Re enhances the fluid velocity. Fig. 3(b) displays that the fluid velocity decelerates by augmenting the effect of the magnetic field. The magnetic field produces the Lorentz force in the hybrid nanofluid flow, and the Lorentz force decreases the drag coefficient in the hybrid nanofluid flow, which diminishes the velocity profiles of the hybrid nanofluid flow for the escalation of M.

Figs. 4(a)-5(d) depict the temperature distribution results affected by the numerous pertinent parameters of the hybrid nanofluid flow involved in the physical assumptions of this analysis. Fig. 4(a) illustrates the physical influence of Reynolds numbers (Re) on the nanofluid flow's thermal profiles. This Figure indicates that the thermal profile is enhanced with a higher Reynolds number because the more significant Reynolds number means the more considerable momentum of the fluid particles. Then, the viscous forces become less dominant in the boundary layer; therefore, the higher momentum of the fluid thickens the thermal boundary layer, enhancing thermal profiles with an increment in Reynolds number. Fig. 4(b) presents the temperature profiles affected by varying the magnetic field parameter (M), which declares that the thermal profiles show dual behavior in the thermal boundary layer for escalating values of the M. Because the applied magnetic field generates the Lorentz force, affecting the drag coefficient. It enhances the

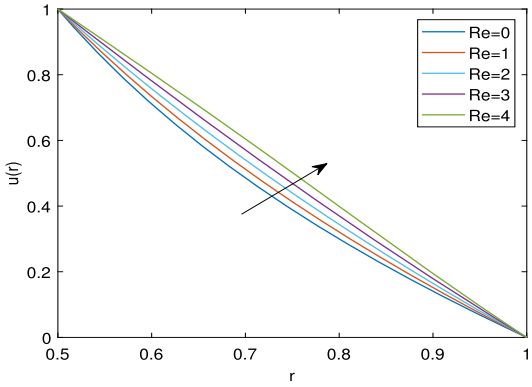

(a) Velocity profiles against Reynolds number

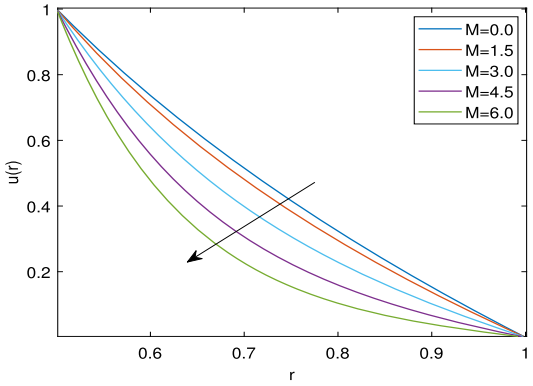

(b) Velocity profiles against magnetic field parameter

Fig. 3. Velocity profiles for the diverse values of Re and M.

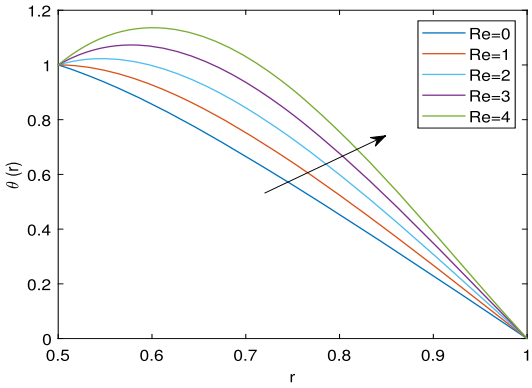

(a) Thermal profiles against Reynolds number

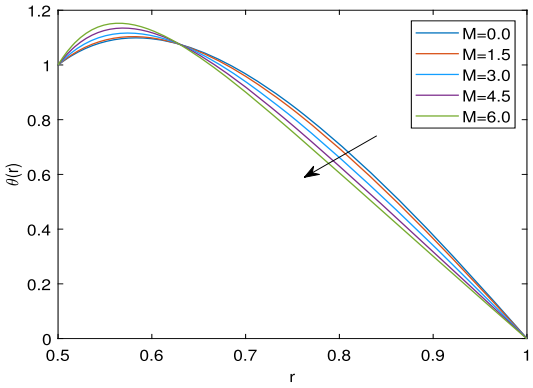

(b) Thermal profiles against magnetic field parameter

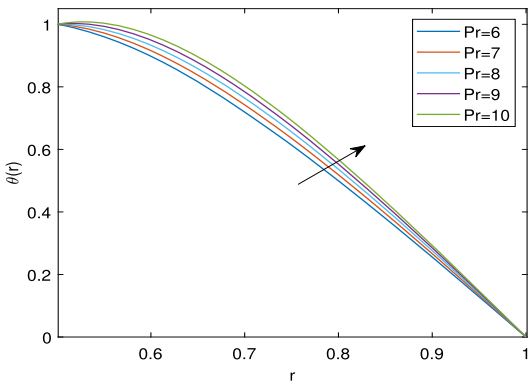

(c) Thermal profiles against Prandtl number

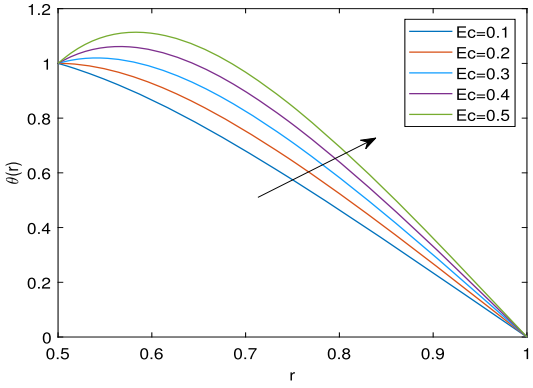

(d) Thermal profiles against Eckert number

Fig. 4. Thermal profiles due to the diverse values of Re, M, Pr, and Ec.

contact between the tube surface and the heat transfer fluid. Therefore, the temperature profile escalates near the surface of external tube, and this effect becomes weak as we move away from the receiver tube surface. Fig. 4(c) presents the response of the Prandtl number (Pr) in the fluid's thermal profile, and it illustrates that the fluid temperature profile grows with the rise in the Prandtl number. The higher Prandtl number indicates that the momentum diffusivity is more dominant, and the more considerable momentum of fluid particles results in higher heat transfer. Fig. 4(d) depicts the thermal profile influenced by the Eckert number (Ec). As per this Figure, the growing Eckert number escalates the thermal profiles. Eckert's number is proportional to the kinetic energy of a hybrid nanofluid. Therefore, increasing kinetic energy enhances the thermal profiles. Fig. 5(a) represents the thermal profiles influenced by the thermophoretic diffusion parameter (Nt), which reports that the thermal profiles are higher for increasing thermophoretic diffusion parameters. Thermophoretic diffusion is the diffusion of nanoparticles owing to the thermal gradient, which enhances the thermal profile. Brownian motion (Nb) effects on the thermal profiles are shown in Fig. 5(a), which declares that the Brownian motion enhances the thermal profile. Because the increasing Brownian motion undergoes more collisions of the nanoparticles, these collisions dissipate more heat to the working fluid. Fig. 5(c) demonstrates the varied thermal profile of hybrid nanofluid by the Lewis number, and the thermal profiles reduce with the rise in Lewis number. Fig. 5(d) picturizes the influence of radiation parameter (Rd) on the thermal profiles, demonstrating that thermal profiles worsen for enhancing the Rd. The trends and behavior of this

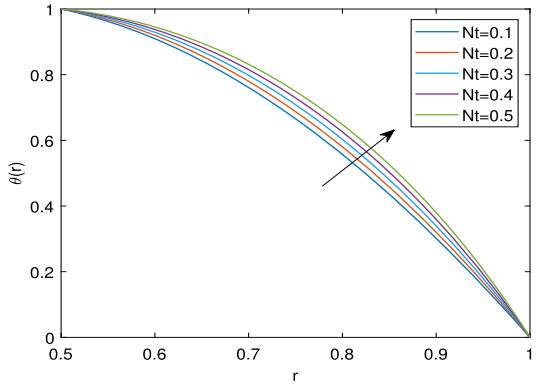

(a) Thermal profiles against thermophoretic diffusion parameter

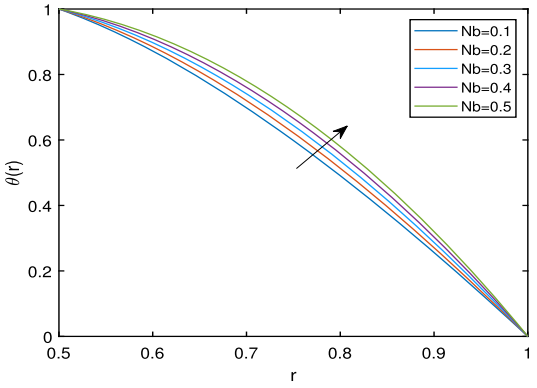

(b) Thermal profiles for the variation in Brownian motion parameter

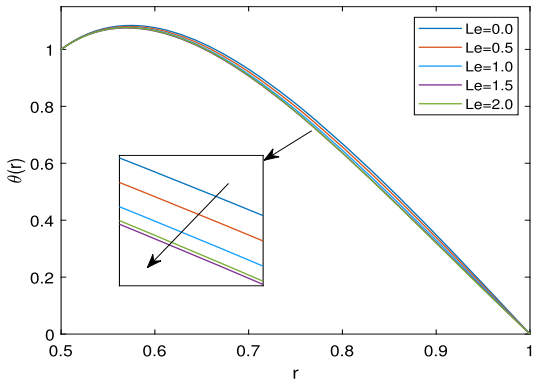

(c) Thermal profiles against Lewis number

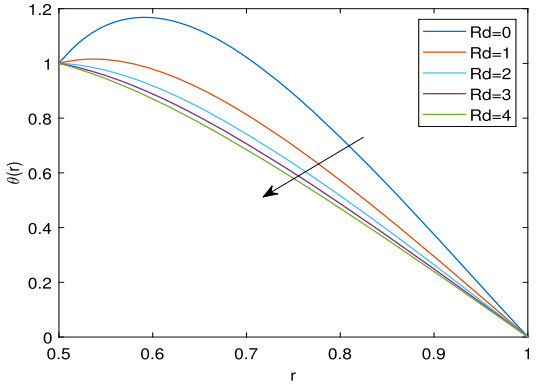

(d) Thermal profiles against radiation parameter

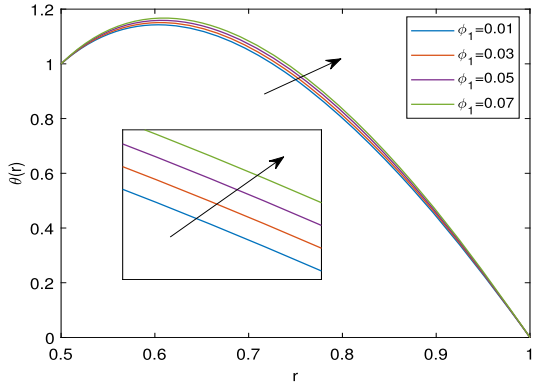

(e) Thermal profiles against Cu nanoparticles volume fraction

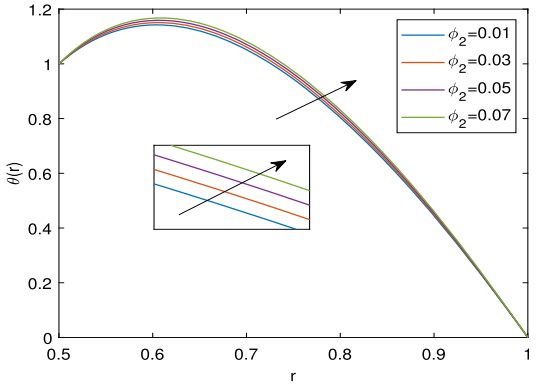

(f) Thermal profiles against $MWCNT$ nanoparticles volume fraction

Fig. 5. Temperature profiles for diverse values of Nt, Nb, Le, Rd, ϕ_1 and ϕ_2.

result are similar to that of the existing literature [49]. Figs. 5(e) and 5(f) present the variations in thermal profiles due to the variation in nanoparticle volume fractions of the Cu nanoparticles and $MWCNT$. This Figure reports that the thermal profiles increases with escalates in the volume fractions of the Cu nanoparticles and $MWCNT$. This happens due to the suspension of nanoparticles in the heat transfer fluid having enhanced physical properties.

5. Quantity of engineering interest

Drag coefficient, heat transfer rate, and mass flow rate are the physical quantities of interest in the fluid flow phenomenon. Moreover, our primary goal here is to improve the performance of solar thermal collectors by enhancing the heat transfer rate at the surface of absorber with heat transfer fluid. Different terminologies are introduced to store thermal energy from incoming solar radiation in more significant amounts to reach sustainable energy requirements. For this purpose, the physical quantity heat transfer rate, i.e., the Nusselt number, is preferable for optimizing heat transfer and absorbing the possibly maximum radiant energy. Mathematically, the Nusselt number is formulated as follows:

$$Nu = -S_4\left(1 + \frac{4Rd}{3S_4}\right)\frac{\partial\theta}{\partial r}|_{r=\eta}$$

In Figs. 6(a)-6(d), Nusselt number (Nu) results are plotted to show the influence of numerous parameters to understand the characteristics of heat transfer in hybrid nanofluid flows with the effect of the rotat-

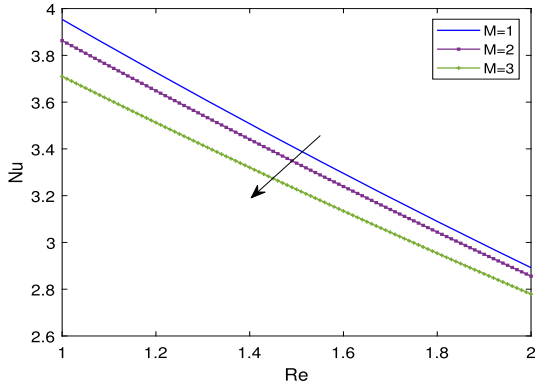

(a) Nusselt number against Reynolds number for distinct values of magnetic field parameter

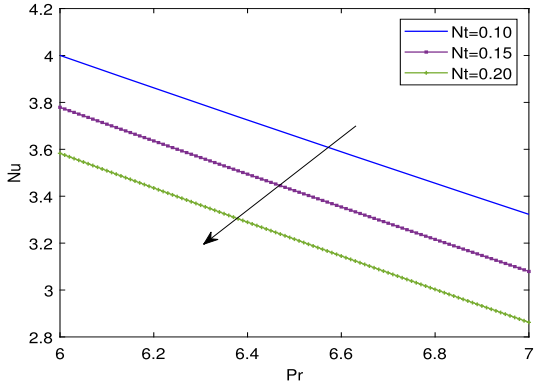

(b) Nusselt number against Prandtl number for distinct values of thermophoretic diffusion parameter

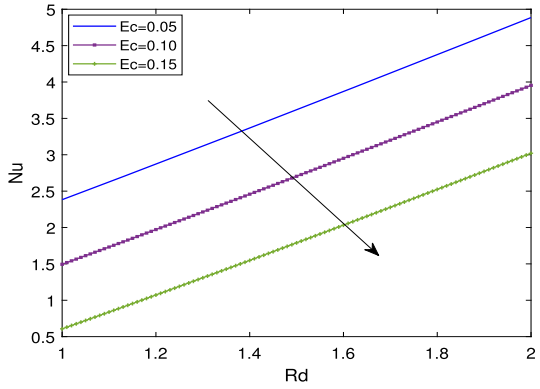

(c) Nusselt number against radiation parameter for distinct values of Eckert number

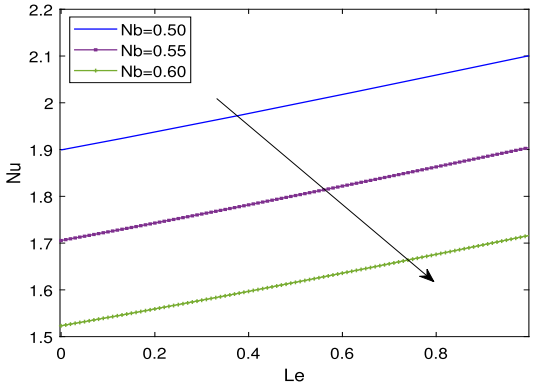

(d) Nusselt number against Lewis number for distinct values of Brownian motion parameter

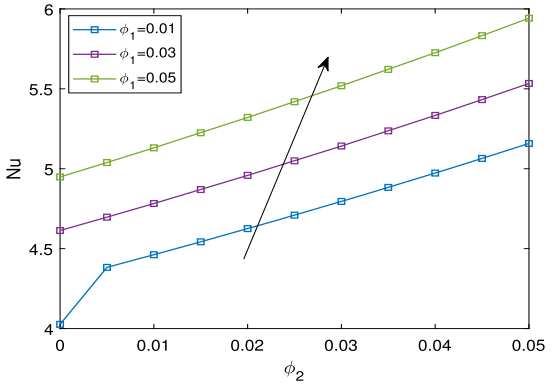

(e) Nusselt number against volume fractions of the hybrid nanoparticle

Fig. 6. Numerical results of the Nusselt number corresponding to the diverse effective physical parameters.

ing tube inside the absorber with thermophoresis and Brownian motion of the nanoparticles in under the impact of the magnetic field. Fig. 6(a) portrays the influence of the Re on the Nu for the different defaults of M, and this shows that the Nu drops with improvement in M and Re. The influence of the Nt and the Pr on the Nu is picturized in Fig. 6(b). This Figure illustrates that a decrement in the Nusselt number is obtained by increasing the thermophoretic diffusion parameter and the Pr. Plot 6(c) picturizes the behavior of the Nu under varying values of the Rd for the different defaults of the Ec. This Plot shows that the Nu increases by escalating the Rd and decreases with an increase in the Ec. Fig. 6(d) illustrates the findings of the Nu against the Lewis number for diverse values of the Nb. The findings of this picture report that the Nu enhances by augmenting the Lewis number and reduces against the improvement in the Nb. Fig. 6(e) illustrates the effect of volume fractions of the Cu nanoparticles and $MWCNT$ on the Nu. This figure shows an enhancement in the Nu for the escalation in volume fractions of the Cu nanoparticles and $MWCNT$.

6. Entropy optimization

Entropy generation is heat loss during an irreversible process in a thermodynamic system. Therefore, it is essential to examine the heat loss during the irreversible process to evaluate the performance of the thermodynamic system. This model generates entropy due to conduc-

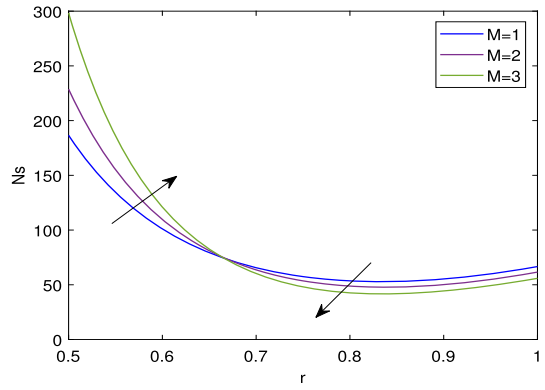

(a) Entropy generation due to magnetic field parameter

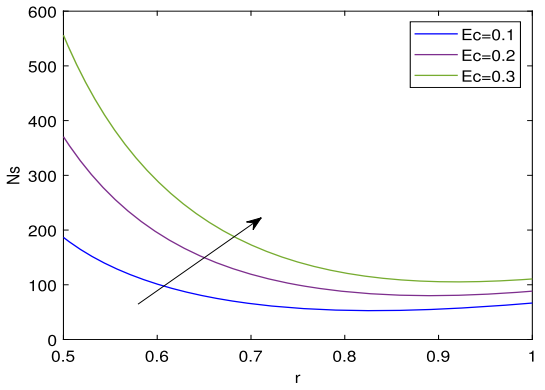

(b) Entropy generation due to Eckert number

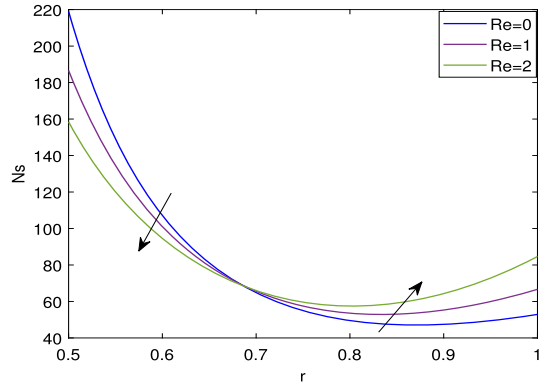

(c) Entropy generation due to Reynolds number

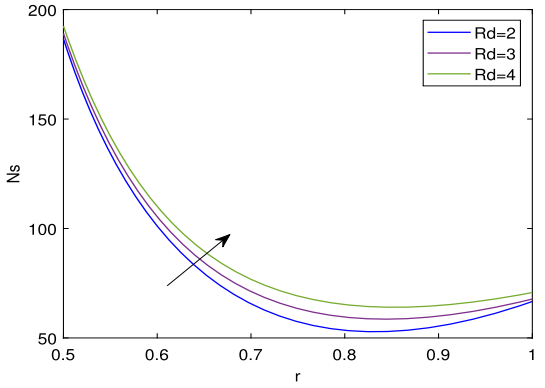

(d) Entropy generation due to radiation parameter

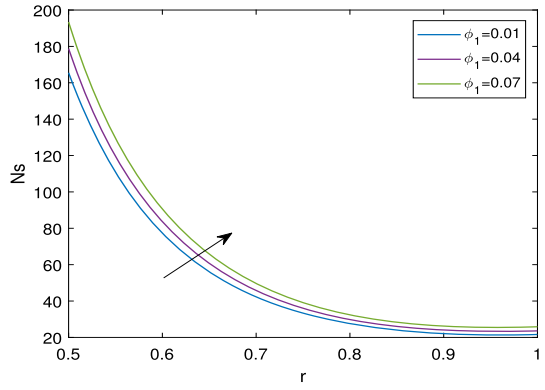

(e) Entropy generation due to volume fraction of Cu nanoparticles

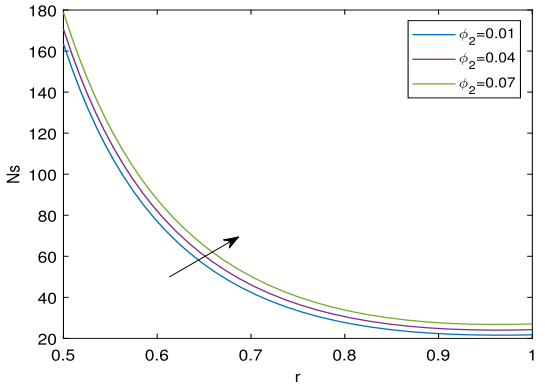

(f) Entropy generation due to volume fraction of $MWCNT$

Fig. 7. Entropy formation due to the various influential physical parameter.

tive heat transfer, viscous dissipation, diffusion of nanoparticles, and magnetic field. Mathematical expression for the entropy generation is given by [50]:

$$E_g = \left(\kappa_{hnf} + \frac{16\sigma^* T_2^3}{3\kappa^*(\rho c_p)_{hnf}}\right)\frac{(\nabla T_f)^2}{(T_2)^2} + \mu_{hnf}\frac{F}{T_2} + \frac{\sigma_{hnf}}{T_2^2}(uB)^2 + RD\frac{(\nabla C_f)^2}{C_2} + RD\frac{\nabla C_f \nabla T_f}{T_2}. \tag{12}$$

$$E_g = \frac{1}{T_2^2}\left(\kappa_{hnf} + \frac{16\sigma^* T_2^3}{3\kappa^*(\rho c_p)_{hnf}}\right)\left(\frac{\partial T}{\partial R}\right)^2 + \frac{\mu_{hnf}}{T_2}\left(\frac{\partial U}{\partial R} - \frac{U}{R}\right)^2 + \frac{\sigma_{hnf}}{(T_2)^2}(UB)^2 + \frac{RD_b}{C_2}\left(\frac{\partial C}{\partial R}\right)^2 + \frac{RD_b}{T_2}\left(\frac{\partial C}{\partial R}\right)\left(\frac{\partial T}{\partial R}\right). \tag{13}$$

Non-dimensionalized form of the expression for the entropy generation after introducing dimensionless variables:

$$N_s = S_4\left(1 + \frac{4Rd}{3S_4}\right)\left(\frac{\partial \theta}{\partial r}\right)^2 + \frac{S_5}{\delta}\frac{M^2}{(1-\eta)^2}PrEc(u^2(r) + \frac{S_2}{\delta}EcPr.. \left(\frac{\partial u}{\partial r} - \frac{1}{r}u\right)^2 + L\frac{\delta_1}{\delta}\left(\frac{\partial \theta}{\partial r}\right)\left(\frac{\partial \phi}{\partial r}\right) + L\left(\frac{\delta_1}{\delta}\right)^2\left(\frac{\partial \phi}{\partial r}\right)^2. \tag{14}$$

Figs. 7(a)-7(d) illustrate the entropy generation (N_s) due to some influential physical parameters for the three different default values of the parameter. Fig. 7(a) shows the behavior of N_s versus the M, which shows that the N_s has dual behavior with the effect of varying the magnetic field strength. The entropy first increases towards the surface of

the inner tube and then changes its behavior at the mid and then decreases towards the surface of the outer tube. The influence of increasing Ec for the variation in N_s is displayed in Fig. 7(b). This Figure shows that the entropy improves by magnifying the Ec. Fig. 7(c) highlights the entropy produced due to the Re, and from this Figure, it is noted that entropy shows dual behavior by varying the Re. N_s first escalates with a growing Re and then decelerates nearly from the middle point of the similarity variable with an increment in the Re. Fig. 7(d) displays the results of N_s affected by the Rd. This Figure reports that entropy increases by enhancing the Rd. Figs. 7(e) and 7(f) represent the influence of nanoparticle volume fractions on the entropy generation. These Figures demonstrate that the escalation of volume fraction for both the nanoparticle Cu and $MWCNT$ enhances the entropy generation.

7. Conclusions

This article investigated the heat transfer and entropy formation in solar collectors due to a rotating tube with thermophoresis and Brownian motion under the effect of the magnetic field. From this study, It is concluded that the fluid velocity is enhanced with the escalation of Re and decelerates with an enhancement in M. The fluid temperature profile increases for the augmented Re, and the temperature profile shows dual behavior for the escalated M; the temperature profile accelerates near the surface of the absorbing tube, and it decelerates away from the surface of the receiver for the increase of the M. Enhancement in Pr, Ec, Nt, and Nb escalates the thermal profiles in the hybrid nanofluid flow. Also, the enhancing nanoparticle concentration increases the thermal profiles. Escalation of the Le and Rd diminishes the thermal profiles. Higher Re, Nt, Pr, M, Nb, and Ec decelerates the Nusselt number. Augmenting the Le, Rd, and nanoparticle concentration enhances the Nusselt number. The contribution of the M in the entropy generation shows dual behavior. Entropy generation first increases with an enhancement in magnetic field parameters and then increases with the increasing effect of the magnetic field. Entropy generation is higher for escalated Ec and Rd values. Augmenting the Re shows dual behavior in the entropy generation, which first escalates with an increment in the Re and then decelerates nearly toward the middle point of the similarity variable with the rise in the Re. The entropy generation is enhanced due to the increase in nanoparticle concentrations of both nanofluids.

CRediT authorship contribution statement

Anup Kumar: Conceptualization, Methodology, Writing – original draft. **Bhupendra K. Sharma:** Formal analysis, Investigation, Methodology, Software. **Taseer Muhammad:** Formal analysis, Supervision, Writing – original draft. **Laura M. Pérez:** Funding acquisition, Supervision, Validation, Writing – review & editing.

Declaration of competing interest

The authors declare that they have no known competing financial interests or personal relationships that could have appeared to influence the work reported in this paper.

Acknowledgement

LMP acknowledges partial financial support from ANID through FONDECYT 1240985. The authors extend their appreciation to the Deanship of Research and Graduate Studies at King Khalid University, KSA for funding this work through Large Research Project under grant number RGP.2/625/45.

References

[1] Padilla RV, Demirkaya G, Goswami DY, Stefanakos E, Rahman MM. Heat transfer analysis of parabolic trough solar receiver. Appl Energy 2011;88(12):5097–110.
[2] Jianfeng L, Jing D, Jianping Y. Heat transfer performance of an external receiver pipe under unilateral concentrated solar radiation. Sol Energy 2010;84(11):1879–87.
[3] Wang F, Shuai Y, Yuan Y, Yang G, Tan H. Thermal stress analysis of eccentric tube receiver using concentrated solar radiation. Sol Energy 2010;84(10):1809–15.
[4] Chen X, Xia X-L, Liu H, Li Y, Liu B. Heat transfer analysis of a volumetric solar receiver by coupling the solar radiation transport and internal heat transfer. Energy Convers Manag 2016;114:20–7.
[5] Lipiński W, Abbasi-Shavazi E, Chen J, Coventry J, Hangi M, Iyer S, et al. Progress in heat transfer research for high-temperature solar thermal applications. Appl Therm Eng 2021;184:116137.
[6] Sattar M, Rehman A, Ahmad N, Mohammad A, Ahmadi AA Al, Ullah N. Performance analysis and optimization of a cooling system for hybrid solar panels based on climatic conditions of Islamabad, Pakistan. Energies 2022;15(17):6278.
[7] Arifin Z, Khairunisa N, Kristiawan B, Prasetyo SD, Bangun WB. Performance analysis of nanofluid-based photovoltaic thermal collector with different convection cooling flow. Civ. Eng. J. 2023;9(8):1922–35.
[8] Sher AA, Ahmad N, Sattar M, Ghafoor U, Shah UH. Effect of various dusts and humidity on the performance of renewable energy modules. Energies 2023;16(13):4857.
[9] Sharma BK, Kumar A, Mishra NK, Albaijan I, Fernandez-Gamiz U. Computational analysis of melting radiative heat transfer for solar riga trough collectors of jeffrey hybrid-nanofluid flow: a new stochastic approach. Case Stud Therm Eng 2023;52:103658.
[10] Prasetyo SD, Budiana EP, Prabowo AR, Arifin Z. Modeling finned thermal collector construction nanofluid-based al2o3 to enhance photovoltaic performance. Civ. Eng. J. 2023;9(12):2989–3007.
[11] Kandasamy R, Muhaimin I, Rosmila A. The performance evaluation of unsteady mhd non-darcy nanofluid flow over a porous wedge due to renewable (solar) energy. Renew Energy 2014;64:1–9.
[12] Sharma B, Sharma M, Gaur R, Mishra A. Mathematical modeling of magneto pulsatile blood flow through a porous medium with a heat source. Int J Appl Mech Eng 2015;20(2):385–96.
[13] Hayat T, Bashir G, Waqas M, Alsaedi A. Mhd 2d flow of Williamson nanofluid over a nonlinear variable thicked surface with melting heat transfer. J Mol Liq 2016;223:836–44.
[14] Dinh MT, Tlili I, Dara RN, Shafee A, Al-Jahmany YYY, Nguyen-Thoi T. Nanomaterial treatment due to imposing mhd flow considering melting surface heat transfer. Phys A: Stat Mech Appl 2020;541:123036.
[15] Mishra A, Sharma B. Mhd mixed convection flow in a rotating channel in the presence of an inclined magnetic field with the hall effect. J Eng Phys Thermophys 2017;90:1488–99.
[16] Hsiao K-L. To promote radiation electrical mhd activation energy thermal extrusion manufacturing system efficiency by using carreau-nanofluid with parameters control method. Energy 2017;130:486–99.
[17] Tripathi B, Sharma BK, Sharma M. Modeling and analysis of mhd two-phase blood flow through a stenosed artery having temperature-dependent viscosity. Eur Phys J Plus 2019;134(9):466.
[18] Soomro FA, Haq RU, Algehyne EA, Tlili I. Thermal performance due to magnetohydrodynamics mixed convection flow in a triangular cavity with circular obstacle. J Energy Storage 2020;31:101702.
[19] Deng Y, Jiang Y, Liu J. Liquid metal technology in solar power generation-basics and applications. Sol Energy Mater Sol Cells 2021;222:110925.
[20] Al-Kouz W, Aissa A, Devi SSU, Prakash M, Kolsi L, Moria H, et al. Effect of a rotating cylinder on the 3d mhd mixed convection in a phase change material filled cubic enclosure. Sustain Energy Technol Assess 2022;51:101879.
[21] Ghandi R, Sharma B, Kumawat C, Beg O, et al. Modeling and analysis of magnetic hybrid nanoparticle (au-al2o3/blood) based drug delivery through a bell-shaped occluded artery with joule heating, viscous dissipation and variable viscosity effects. Proc Inst Mech Eng, E J Process Mech Eng 2022.
[22] Khanduri U, Sharma BK, Sharma M, Mishra NK, Saleem N. Sensitivity analysis of electroosmotic magnetohydrodynamics fluid flow through the curved stenosis artery with thrombosis by response surface optimization. Alex Eng J 2023;75:1–27.
[23] Sharma B, Gandhi R. Combined effects of joule heating and non-uniform heat source/sink on unsteady mhd mixed convective flow over a vertical stretching surface embedded in a darcy-forchheimer porous medium. Propuls Power Res 2022;11(2):276–92.
[24] Sharma BK, Kumar A, Gandhi R, Bhatti MM, Mishra NK. Entropy generation and thermal radiation analysis of emhd jeffrey nanofluid flow: Applications in solar energy. Nanomaterials 2023;13(3):544.
[25] Kumar A, Sharma BK, Gandhi R, Mishra NK, Bhatti M. Response surface optimization for the electromagnetohydrodynamic cu-polyvinyl alcohol/water jeffrey nanofluid flow with an exponential heat source. J Magn Magn Mater 2023;576:170751.
[26] Gandhi R, Sharma BK, Kumar A, Almohsen B, Fernandez-Gamiz U. Entropy generation optimization of emhd mixed convective flow with higher order chemical reaction: Sensitivity analysis. Case Stud Therm Eng 2024;54:104079.
[27] Ahmadi N. Influences of optimizing the turbulator arrangement on the heat transfer and hydraulic characteristics of the tubular heat exchanger. Int J Therm Sci 2024;197:108792.
[28] Ji J, Ni X, Shi B, Pan Y, Liu P. Influence of deflector direction on heat transfer capacity of spiral elastic tube heat exchanger. Appl Therm Eng 2024;236:121754.
[29] Ghasemi SE, Hatami M, Jing D, Ganji D. Nanoparticles effects on mhd fluid flow over a stretching sheet with solar radiation: A numerical study. J Mol Liq 2016;219:890–6.

[30] Anbuchezhian N, Srinivasan K, Chandrasekaran K, Kandasamy R. Thermophoresis and brownian motion effects on boundary layer flow of nanofluid in presence of thermal stratification due to solar energy. Appl Math Mech 2012;33:765–80.
[31] Kandasamy R, Muhaimin I, Mohamad R. Thermophoresis and brownian motion effects on mhd boundary-layer flow of a nanofluid in the presence of thermal stratification due to solar radiation. Int J Mech Sci 2013;70:146–54.
[32] Shehzad SA, Hayat T, Alsaedi A, Obid MA. Nonlinear thermal radiation in the three-dimensional flow of jeffrey nanofluid: a model for solar energy. Appl Math Comput 2014;248:273–86.
[33] Patel HR, Singh R. Thermophoresis, brownian motion and non-linear thermal radiation effects on mixed convection mhd micropolar fluid flow due to nonlinear stretched sheet in porous medium with viscous dissipation, joule heating and convective boundary condition. Int Commun Heat Mass Transf 2019;107:68–92.
[34] Nayak M, Hakeem AA, Ganga B, Khan MI, Waqas M, Makinde OD. Entropy optimized mhd 3d nanomaterial of non-newtonian fluid: a combined approach to good absorber of solar energy and intensification of heat transport. Comput Methods Programs Biomed 2020;186:105131.
[35] Rekha M, Sarris IE, Madhukesh J, Raghunatha K, Prasannakumara B. Impact of thermophoretic particle deposition on heat transfer and nanofluid flow through different geometries: An application to solar energy. Chin J Phys 2022;80.
[36] Sharma B, Kumar A, Gandhi R, Bhatti M. Exponential space and thermal-dependent heat source effects on electro-magneto-hydrodynamic jeffrey fluid flow over a vertical stretching surface. Int J Mod Phys B 2022;36(30):2250220.
[37] Bejan A. Fundamentals of exergy analysis, entropy generation minimization, and the generation of flow architecture. Int J Energy Res 2002;26(7).
[38] Böer KW, Tamm G. Solar conversion under consideration of energy and entropy. Sol Energy 2003;74(6):525–8.
[39] Oztop HF, Al-Salem K. A review on entropy generation in natural and mixed convection heat transfer for energy systems. Renew Sustain Energy Rev 2012;16(1):911–20.
[40] Guelpa E, Sciacovelli A, Verda V. Entropy generation analysis for the design improvement of a latent heat storage system. Energy 2013;53:128–38.
[41] Khan NS, Kumam P, Thounthong P. Renewable energy technology for the sustainable development of thermal system with entropy measures. Int J Heat Mass Transf 2019;145:118713.
[42] Said Z, Ghodbane M, Sundar LS, Tiwari AK, Sheikholeslami M, Boumeddane B. Heat transfer, entropy generation, economic and environmental analyses of linear fresnel reflector using novel rgo-co3o4 hybrid nanofluids. Renew Energy 2021;165:420–37.
[43] Sharma B, Gandhi R, Mishra NK, Al-Mdallal QM. Entropy generation minimization of higher-order endothermic/exothermic chemical reaction with activation energy on mhd mixed convective flow over a stretching surface. Sci Rep 2022;12(1):1–18.
[44] Gandhi R, Sharma BK, Makinde OD. Entropy analysis for mhd blood flow of hybrid nanoparticles (au–al2o3/blood) of different shapes through an irregular stenosed permeable walled artery under periodic body acceleration: Hemodynamical applications. J Appl Math Mech (Z Angew Math Mech) 2022:e202100532.
[45] Kumawat C, Sharma B, Al-Mdallal QM, Rahimi-Gorji M. Entropy generation for mhd two phase blood flow through a curved permeable artery having variable viscosity with heat and mass transfer. Int Commun Heat Mass Transf 2022;133:105954.
[46] Tavakoli A, Farzaneh-Gord M, Ebrahimi-Moghadam A. Using internal sinusoidal fins and phase change material for performance enhancement of thermal energy storage systems: Heat transfer and entropy generation analyses. Renew Energy 2023;205:222–37.
[47] Widjaja RG, Asrol M, Agustono I, Djuana E, Harito C, Elwirehardja G, et al. State of charge estimation of lead acid battery using neural network for advanced renewable energy systems. Emerg Sci J 2023;7(3):691–703.
[48] Sharma BK, Kumar A, Almohsen B, Fernandez-Gamiz U. Computational analysis of radiative heat transfer due to rotating tube in parabolic trough solar collectors with darcy forchheimer porous medium. Case Stud Therm Eng 2023;51:103642.
[49] Mohsenian S, Gouran S, Ghasemi S. Evaluation of weighted residual methods for thermal radiation on nanofluid flow between two tubes in presence of magnetic field. Case Stud Therm Eng 2022;32:101867.
[50] Kumar A, Sharma BK, Bin-Mohsen B, Fernandez-Gamiz U. Statistical analysis of radiative solar trough collectors for mhd jeffrey hybrid nanofluid flow with gyrotactic microorganism: entropy generation optimization. Int J Numer Methods Heat Fluid Flow 2024.